In-plane heterostructures of graphene and hexagonal boron nitride with controlled domain sizes

Zheng Liu[1], Lulu Ma[1], Gang Shi[1], Wu Zhou[2,3], Yongji Gong[1], Sidong Lei[1], Xuebei Yang[4], Jiangnan Zhang[1], Jingjiang Yu[5], Ken P. Hackenberg[1], Aydin Babakhani[4], Juan-Carlos Idrobo[3], Robert Vajtai[1], Jun Lou[1]* and Pulickel M. Ajayan[1]*

Graphene and hexagonal boron nitride (h-BN) have similar crystal structures with a lattice constant difference of only 2%. However, graphene is a zero-bandgap semiconductor with remarkably high carrier mobility at room temperature[1-3], whereas an atomically thin layer of h-BN[4-9] is a dielectric with a wide bandgap of ∼5.9 eV. Accordingly, if precise two-dimensional domains of graphene and h-BN can be seamlessly stitched together, hybrid atomic layers with interesting electronic applications could be created[10]. Here, we show that planar graphene/h-BN heterostructures can be formed by growing graphene in lithographically patterned h-BN atomic layers. Our approach can create periodic arrangements of domains with size ranging from tens of nanometres to millimetres. The resulting graphene/h-BN atomic layers can be peeled off the growth substrate and transferred to various platforms including flexible substrates. We also show that the technique can be used to fabricate two-dimensional devices, such as a split closed-loop resonator that works as a bandpass filter.

Graphene/h-BN hybrid structures can exist in various configurations, one of which is a vertically stacked graphene and h-BN heterostructure superlattice[10–16]. We have shown previously that such heterostructures can be grown using a two-step chemical vapour deposition (CVD) method in which h-BN is grown on graphene[16]. An alternative configuration of these hybrid structures is an in-plane graphene/h-BN atomic layer in which the two materials are seamlessly integrated into a lateral heterostructure[10]. In-plane graphene/h-BN heterostructures with randomly distributed domains can be synthesized with CVD using a mixed carbon (CH_4) and h-BN (ammonia borane) source (Supplementary Fig. S1)[17]. However, the fabrication of novel electronic devices will require the size and shape of the different domains to be engineered precisely.

Figure 1a presents a schematic illustration of the steps in the fabrication of planar graphene/h-BN structure landscapes with controlled domain shapes at larger sizes (millimetre range). The h-BN films were synthesized using the CVD method with ammonia borane (NH_3-BH_3) powder as the precursor and copper/nickel foils as the substrates (see Methods)[18]. The as-prepared h-BN was partially etched with exposed regions defined by laser-cut masks. Few-layer graphene was grown on the etched regions at 1,000 °C using CH_4 (4 s.c.c.m.) as the carbon source and Ar/H_2 as carrier gas. Figure 1b shows a photo of an as-prepared graphene/h-BN

sample on a copper foil. The various patterns (comb, bars and rings) with darker contrast are graphene, and the remaining areas are covered by h-BN. Figure 1c shows a graphene/h-BN comb structure floating in deionized (DI) water after coating with poly(methyl methacrylate) (PMMA) as a supporting layer and etching away the copper substrate using 10% HNO_3. A scanning electron microscopy (SEM) image of a graphene ring structure surrounded by h-BN regions is shown in Fig. 1d, where the light regions are graphene and the dark regions correspond to h-BN. With h-BN as the supporting matrix, the as-prepared graphene/h-BN devices can be transferred to any arbitrary substrate, including silica (Fig. 1e) or polydimethylsiloxane (PDMS) (Fig. 1f), and the whole film containing heterostructure domains remains mechanically intact during transfer from the growth substrate.

To fabricate the graphene/h-BN patterns with smaller feature sizes, photolithography was used to produce masks in various patterns for subsequent argon ion etching, as shown in Figure 2. Figure 2a,d presents SEM images of a sketch of an owl (the symbol of Rice University) and an array of circles, made from graphene in plane with h-BN. Heterostructures with other patterns have also been fabricated, as shown in Supplementary Fig. S2. The darker regions in these SEM images are h-BN layers. Figure 2b,e presents the corresponding optical images, in which graphene is in purple and h-BN in light blue. The thickness of the h-BN layer is controlled by the growth conditions to be less than 2 nm, and similarly for the graphene layers (Supplementary Fig. S3). Fracture was rarely observed at the interface between the graphene and h-BN, even after transferring the graphene/h-BN films to other substrates, demonstrating good interfacial continuity between the different landscapes. Figure 2c,f shows Raman maps of the corresponding patterns using the graphene 2D Raman peak at ∼2,700 cm^{-1}. Figure 2g,h presents SEM images of alternating stripes of graphene/h-BN (width of each line, ∼10 μm). Photolithography and argon ion etching can produce a feature size on the graphene/h-BN landscape as small as a few micrometres, whereas the focused ion beam (FIB) method provides an alternative direct etching method for the creation of nanoscale patterns, feasibly generating line features as small as ∼100 nm (Fig. 2i, Supplementary Fig. S4).

To characterize the interface between graphene and h-BN, Raman spectroscopy, atomic force microscopy (AFM) and aberration-corrected scanning transmission electron microscopy (STEM) were used. Figure 3a shows the Raman spectra collected

[1]Department of Mechanical Engineering and Materials Science, Rice University, Houston, Texas 77005, USA, [2]Department of Physics and Astronomy, Vanderbilt University, Nashville, Tennessee 37235, USA, [3]Materials Science and Technology Division, Oak Ridge National Laboratory, Oak Ridge, Tennessee 37831, USA, [4]Department of Electrical and Computer Engineering, Rice University, Houston, Texas 77005, USA, [5]Nanotechnology Measurements Division, Agilent Technologies, 4330. W. Chandler Boulevard, Chandler, Arizona 85226, USA. *e-mail: ajayan@rice.edu; jlou@rice.edu
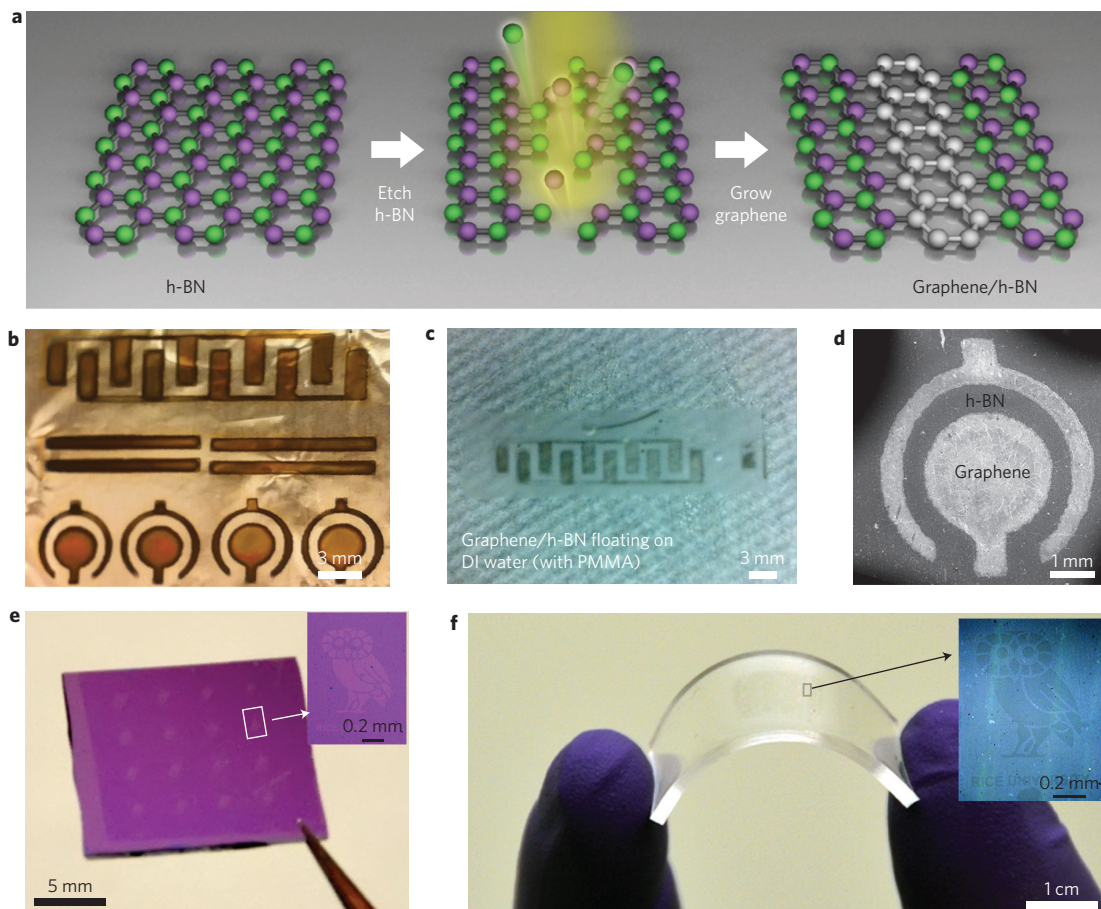
Figure 1 | Creation of millimetre-sized graphene/h-BN in-plane heterostructures. a, Illustration of the fabrication procedure for in-plane graphene/h-BN heterostructures. Steps: preparation of h-BN films using the CVD method; partial etching of h-BN by argon ions to give predesigned patterns; subsequent CVD growth of graphene on the etched regions. **b,** Optical image of the as-grown graphene/h-BN patterned layers (shaped as combs, bars and rings) on a copper foil. Light areas are h-BN and dark areas are graphene. **c,** Optical image of a graphene/h-BN film separated from copper, on water, after coating with PMMA and etching the copper foil. **d,** SEM image showing an h-BN ring surrounded by graphene. **e,f,** Graphene/h-BN owl patterns that have been transferred on silica and PDMS, respectively. Insets: optical images of individual owls.

from the graphene layers, h-BN layers, and also their interface. In the graphene and h-BN regions (indicated by black and blue arrows, respectively), the Raman spectra can be identified perfectly as pure graphene and h-BN. In the h-BN regions, vibration mode E_{2g} was observed, but no peaks from the carbon dopant (D or G peak) were detected, suggesting that there were no carbon impurities doped into the h-BN lattice during the growth of graphene. Furthermore, all the intrinsic vibration modes from both h-BN and graphene could be found at their interface. A further examination of the interface was performed by AFM, as shown in Fig. 3c,d. Figure 3b shows an optical image of the graphene/h-BN alternating striped film used for AFM characterizations. The height topography and corresponding current-sensing image are shown in Fig. 3c,d, respectively. The height difference between the graphene and h-BN regions is barely noticeable (Fig. 3c, inset), but the graphene and h-BN can be differentiated in the current-sensing image. STEM imaging and elemental analysis with electron energy-loss spectroscopy (EELS) provided us with more detail about the interface, as shown in Fig. 3e–h and Supplementary Figs S5–S7. The graphene and h-BN regions are difficult to differentiate under conventional transmission electron microscopy (TEM), but annular dark-field (ADF) STEM imaging provides a better way to show the difference in contrast for the layers (Supplementary Fig. S6a,b). Figure 3e shows a STEM-ADF image of the h-BN/graphene interface (slight variation in thickness can be

quantified via the image intensity; Supplementary Fig. S5). The bright contrast in the graphene region originates from the polymer residuals and hydrocarbon contaminations produced during TEM sample preparation. The interface can be more clearly observed using EELS. Figure 3f,g shows the EELS boron and nitrogen spectrum imaging maps for the entire area shown in Fig. 3e. Indeed, a sharp lateral interface between the h-BN and graphene layers can be observed in these maps. The intensity line profile (Fig. 3f, inset) of the boron map across the interface further shows that the sharpness of the graphene/h-BN interface is within 1 nm, corresponding to a single pixel in the line scan. The average N/B ratio from the whole h-BN region is quantified to be 1.1 ± 0.1 from the EEL spectrum, confirming the stoichiometry of the h-BN film. The detailed atomic structure of the graphene/h-BN interface is shown in Fig. 3h in a STEM bright-field image, with the position of the interface highlighted by a dashed line. The lattice fringes from the h-BN layer are clearly visible, although the presence of polymer residuals makes it difficult to directly resolve the lattice of graphene from the image. However, the fast Fourier transform (FFT) pattern (Fig. 3i) of the image shows the diffraction spots from both graphene and h-BN. The dashed circle in Fig. 3i marks the 2.13 Å spacing of graphene, and the six h-BN spots can be identified inside the graphene ring.

To further confirm that the graphene and h-BN are grown contiguously in the same plane, depth profiles were obtained
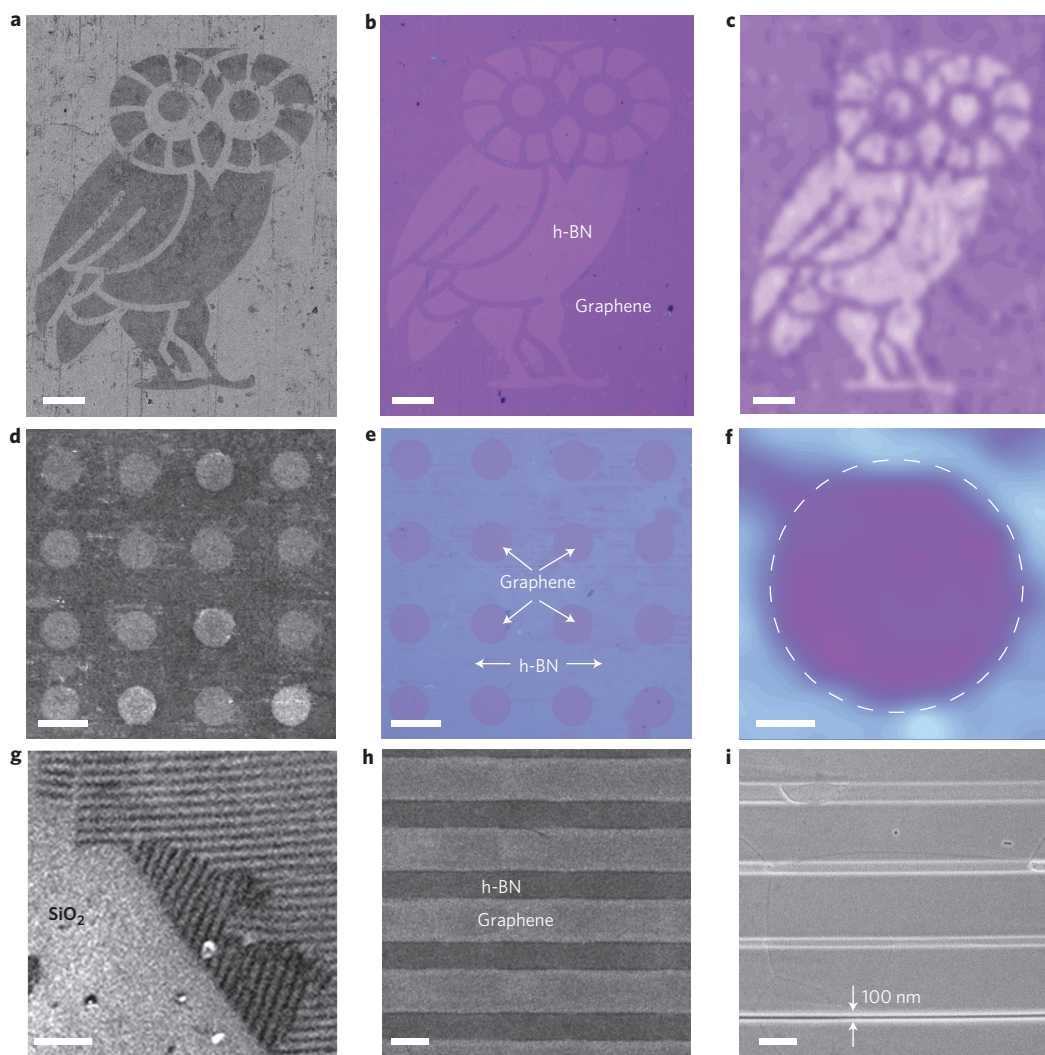
Figure 2 | Creation of micro- to nanoscale patterned graphene/h-BN in-plane heterostructures. a–c, SEM image, optical image and Raman mapping of micrometre-sized owl pattern (symbol of Rice University). Scale bars, 100 μm. The owl contour is designed in h-BN, and the remainder is graphene. Raman mapping is performed with the 2D peak of graphene at ~2,700 cm^{-1}. **d–f**, SEM image, optical image and Raman mapping of a graphene/h-BN array of circles, with graphene circles embedded in an h-BN matrix. Scale bars, 50 μm (**d**), 50 μm (**e**) and 10 μm (**f**). **g,h**, SEM images of graphene/h-BN stripes. Scale bars, 50 μm (**g**) and 10 μm (**h**). **i**, SEM image of graphene/h-BN strip structure with graded strip dimensions, fabricated by FIB etching of h-BN and subsequent graphene growth. The widths of each strip, from top to bottom, are 1 μm, 500 nm, 200 nm and 100 nm, respectively. Scale bar, 1 μm.

using X-ray photoelectron spectroscopy (XPS) at the in-plane graphene/h-BN structure (Supplementary Fig. S8), and the results were compared with those for vertically stacked graphene/h-BN (which we have published previously[16]). The XPS depth profile was obtained by alternating sputtering of the sample (layer-by-layer) and collecting XPS spectra, to provide the distribution of elements in the z-direction. For the vertically stacked graphene/h-BN structure (Supplementary Fig. S8e), the intensity of carbon increased slightly during the first few sputtering processes due to the removal of the top BN layers, and then decreased when part of the graphene layer began to be etched away. In contrast, for the graphene/h-BN heterostructure developed in this study (Supplementary Fig. S8d), the intensities for all elements (boron, nitrogen and carbon) decreased monotonically, confirming the in-plane distribution of all elements, that is, the formation of a lateral graphene/h-BN lateral heterostructure.

To evaluate the impact of the lithographically defined graphene/h-BN structure on device transport properties, field-effect transistor (FETs) devices were fabricated based on a film composed of alternative stripes of pristine graphene and graphene/h-BN (Fig. 4a–c).

The applied source–drain voltage was 1 mV. The insets show the linear I–V characteristics obtained at zero gate, as well as a schematic of the devices. Device mobility was estimated to be $\mu = (dI_{ds}/dV_g) \times [L/(WC_iV_{ds})]$ (ref. 19), where L is the channel length (~100 μm), W is the channel width (~10 μm) and C_i is the areal capacitance per unit area between the channel and back-gate (~1.2×10^{-8} F cm^{-2}). The mobilities in Fig. 4a,b are ~1,700 and 520 cm^2 V^{-1} s^{-1}, respectively. For the pristine graphene and graphene/h-BN FETs (Fig. 4a,b), we obtained comparable mobilities (ranging from ~190 to 2,000 cm^2 V^{-1} s^{-1}) for various devices. No gating effect was observed for the graphene/h-BN FETs with current flowing perpendicular to the stripes (Fig. 4c).

Although versatile and high-performance graphene/h-BN electronics have been demonstrated, devices using such heterostructures require complex and challenging multistep fabrication processes. Our approach of creating in-plane graphene/h-BN interfaces introduces a new approach to integrating two-dimensional heterostructures into device architectures. Such devices could be 'grown' in a furnace with seamless integration of graphene and h-BN into rational engineered atomic layers, and then transferred onto
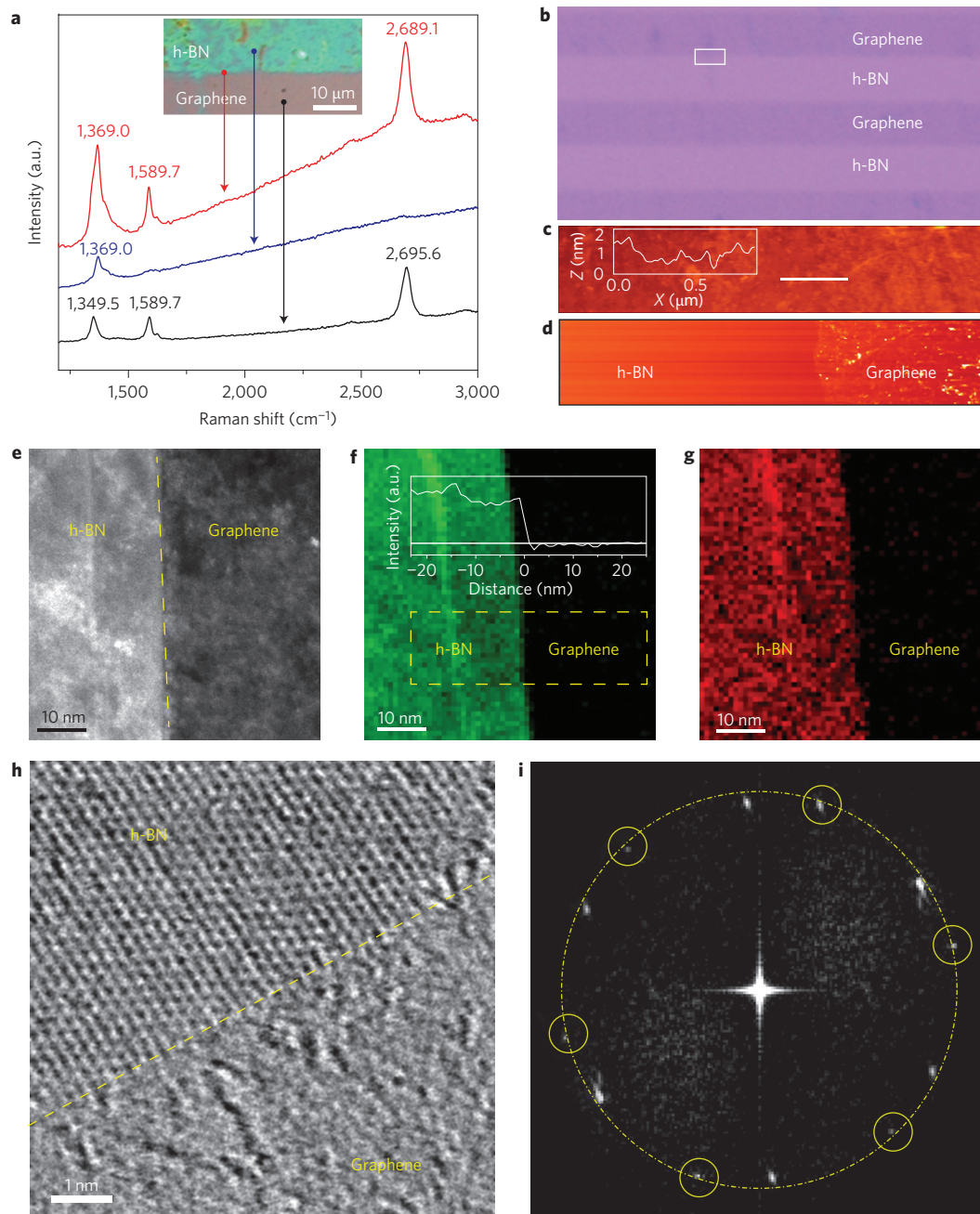
Figure 3 | Raman, AFM and TEM characterization of graphene/h-BN interfaces. a, Raman spectra collected at the graphene, h-BN and their interface in a graphene/h-BN film. **b**, Optical image of alternating stripes of graphene and h-BN. **c,d**, AFM height topography and corresponding current-sensing image of the graphene and h-BN interface from the area indicated in **b**. Inset (**c**): height profile. **e**, STEM-ADF image showing the graphene/h-BN interface. The left part is h-BN and the right is graphene. **f,g**, EELS mapping of boron and nitrogen from the area shown in **e**. Inset (**f**): intensity profile along the trajectory in the dashed box, showing the sharp interface between the h-BN and graphene. **h**, STEM bright field (BF) imaging of the graphene/h-BN interface, highlighted by the dashed line. **i**, Corresponding FFT diffraction patterns showing the diffraction spots from graphene and h-BN. The dashed circle marks the 2.13 Å spacing of graphene.

arbitrary substrates. This approach makes it possible to fabricate fully hybrid two-dimensional structures that could act as fully functional devices. As a demonstration, we fabricated a graphene/h-BN split closed-loop resonator (Fig. 4d–f; Supplementary Figs S9–S11), with h-BN serving as an insulating dielectric matrix for the active graphene component, all fabricated in-plane. An optical image of the device is shown in the inset to Fig. 4d. The flexibility of the graphene/h-BN atomic-layer devices, as a result of their extraordinary mechanical properties[18,20], makes these two-dimensional devices very attractive for flexible electronic applications.

We further characterized the high-frequency response of this resonator using an Agilent N5230C PNA Microwave Network Analyzer. The measured results for the insertion ($|S_{21}|$) and return loss ($|S_{11}|$) are shown in Fig. 4d. The resonating frequency is located at ~1.95 GHz, a value close to the value for copper microstrips with similar geometries[21,22]. This can be understood, as the resonator can be modelled as a serial RLC circuit. The resonance frequency is determined by the equivalent inductance L and capacitance C according to $1/[2\pi\sqrt{(LC)}]$. The results for the equivalent RLC circuit are shown in Fig. 4e,f. S_{43} and S_{33} are calculated
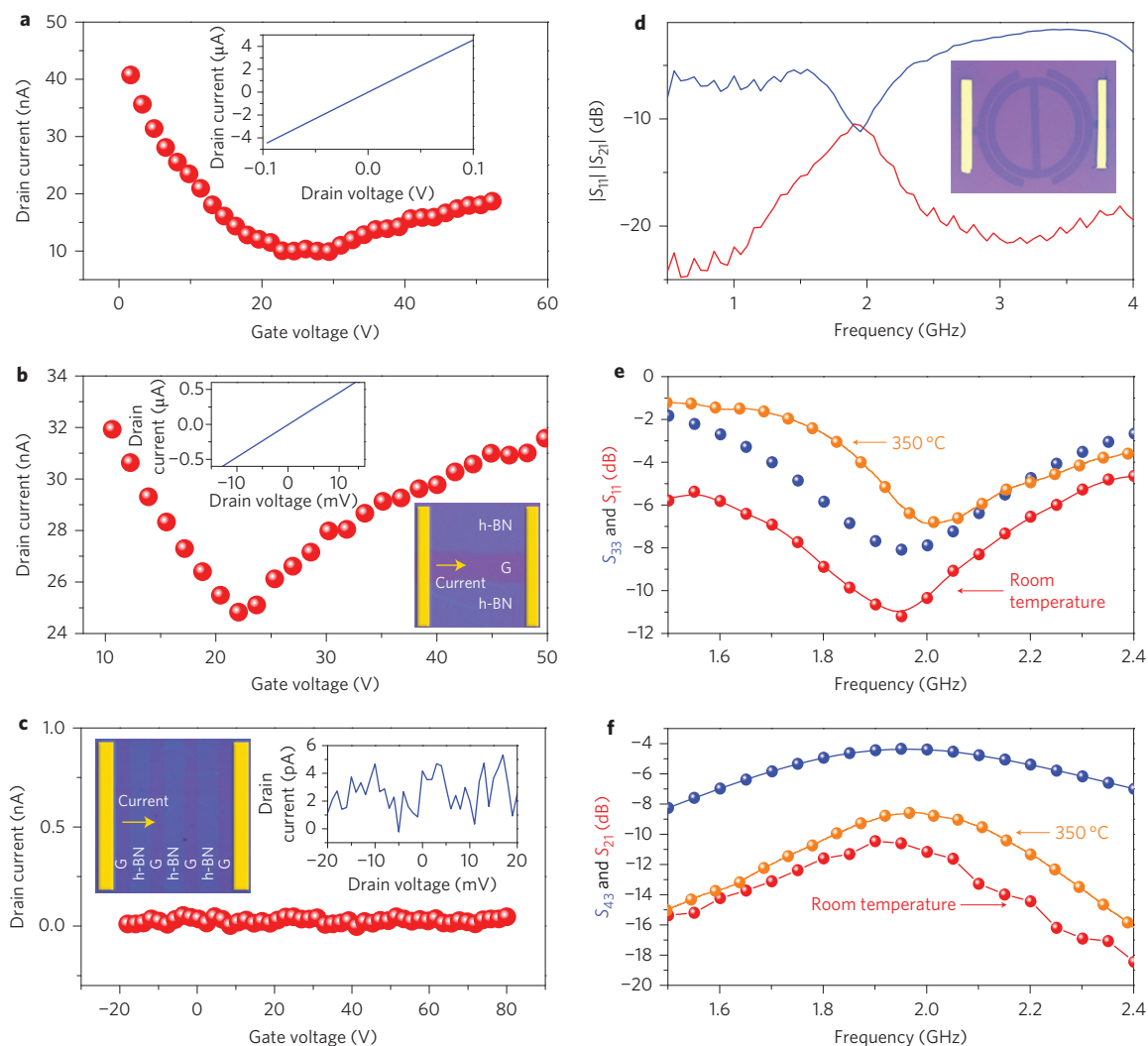
Figure 4 | Graphene/h-BN FET and split closed-loop resonator. a–c, Electrical measurements of pristine graphene and graphene/h-BN stripe FET devices: pristine graphene-based FET (**a**); graphene/h-BN FET with current flowing along the graphene stripes (**b**). **c,** Graphene/h-BN FET with current flowing perpendicular to the stripes. Insets: current–voltage behaviour and schematics of the devices. **d–f,** Radio frequency (RF) measurements of graphene/h-BN-based split closed-loop resonator. Plot of insertion ($|S_{21}|$) and return ($|S_{11}|$) loss versus frequency (**d**). Inset: optical image of the two-dimensional graphene/h-BN layer resonator. Size, ~3 cm × 3 cm. Insertion (**e,** S_{21} and S_{43}) and return (**f,** S_{11} and S_{33}) loss versus frequency. Blue curves are calculated results. Red and orange curves are experimental results at room temperature and 350 °C, respectively.

results (blue), and S_{21} and S_{11} are experimental results (red and orange). The fitting values are as follows: $R = 65\ \Omega$, $L = 30\ \text{nH}$ and $C = 220\ \text{fF}$. We noticed that the shapes of the calculated S parameter versus frequency are very similar for both S_{11} and S_{21}. The devices were measured from room temperature to 350 °C, and showed similar behaviours at all temperatures. Compared with conventional metal-based microstrips[21–23], such graphene/h-BN microstrips can serve as active and transfer-ready atomic layers for the fabrication of both compact and flexible microwave components, such as bandpass filters, couplers, antennas and so on. Furthermore, carefully engineered hybrid atomic layers incorporating both metal and dielectric components, such as this graphene/h-BN resonator, are also a good supplement to many other graphene devices, including amplifiers, multipliers and mixers[24,25] for high-frequency applications.

In conclusion, we have demonstrated the creation of graphene and h-BN in-plane heterostructures with controlled domain sizes by using lithography patterning and sequential CVD growth steps. Feature sizes as small as 100 nm can be fabricated using this approach. Importantly, the shapes of the graphene and h-BN

domains can be controlled precisely, and sharp graphene/h-BN interfaces can be created. Through the appropriate combination of different two-dimensional layers, entire devices could be engineered in a single atomic layer. Such hybrid structures will pave the way for the development of future flexible two-dimensional electronic and optical devices[26].

Methods

MF319. With masks covering h-BN films, the Phantom III Reactive Ion Etch (RIE) System was used to etch graphene/h-BN samples with argon ions. The power and argon flow rate were 100 W and 10 s.c.c.m., respectively. The reaction time ranged from 10 to 60 s depending on the thickness of the h-BN. The photoresist on the copper foil was removed with acetone and Remover PG. We noticed that a longer etching time made it hard to remove the photoresist. A FIB system (FEI 235 Dual-Beam) was also used to pattern samples without using masks, giving a feature size as small as 100 nm. The beam current was ~40 pA.

The etched samples were transferred to another CVD furnace for the growth of graphene. To grow graphene, the temperature was first raised to 950 °C with 10 torr Ar/H_2 gas flow. The Ar/H_2 gas was cut off when the temperature reached 950 °C, and 4 s.c.c.m. CH_4 was introduced into quartz for ~10 min for growth of the graphene. A fast annealing process was carried out at a rate of 50 °C min^{-1} under the protection of a 500 mtorr Ar/H_2 atmosphere. The as-grown graphene/h-BN split closed-loop resonator was transferred onto the SiO_2/silicon substrate. Gold/titanium (30 nm/4 nm) electrodes were deposited on both leads of the graphene (Fig. 4a), then connected to SubMiniature version A (SMA) connectors for high-frequency measurements. Calibrations were performed using the standard cal-kit before measurements.

The bottom-gated graphene and graphene/h-BN FETs were first transferred onto a SiO_2/Si (285 nm) wafer, and chromium/gold (3 nm/40 nm) electrodes were pre-patterned on them using photolithography. The FET devices were measured at a probe station (Desert Cryogenic TT-probe 6 system) under vacuum (1×10^{-5} to 1×10^{-6} torr) connected to an Agilent 4155C semiconductor parameter analyser.

Characterizations of graphene/h-BN heterostructures. A field-emission SEM (JEOL 6500F) was used to characterize the morphology of the graphene/h-BN samples. Raman spectroscopy (Renishaw inVia) was used for sample analysis with 514.5 nm laser excitation. For Raman mapping, a total of 3,456 spectra (15 μm spacing) were collected for Fig. 2c and 225 Raman spectra (4 μm spacing) for Fig. 2f. XPS (PHI Quantera) was used for chemical analysis of the samples using monochromatic aluminium Kα X-rays. Depth profiles were performed with an accelerated-voltage 3 kV argon ion beam and an alternative mode within an etching area of 2 nm × 2 mm to etch the graphene/h-BN films. MultiPak software was used for the data analyses. AFMs (Agilent PicoScan 5500 and Veeco Digital Instrument Nanoscope IIIA) were used to obtain film thicknesses and topographical variations of the samples. The STEM experiments were performed with an aberration-corrected Nion UltraSTEM, operating at 60 kV (ref. 27). EEL spectra were collected using a Gatan Enfina spectrometer, with an EELS collection semi-angle of 48 mrad. The convergence semi-angle for the incident probe was 31 mrad. ADF images were collected for a half-angle range of ~86–200 mrad.

References

1. Novoselov, K. S. *et al.* Electric field effect in atomically thin carbon films. *Science* **306,** 666–669 (2004).
2. Li, X. *et al.* Large-area synthesis of high-quality and uniform graphene films on copper foils. *Science* **324,** 1312–1314 (2009).
3. Chen, J-H., Jang, C., Xiao, S., Ishigami, M. & Fuhrer, M. S. Intrinsic and extrinsic performance limits of graphene devices on SiO_2. *Nature Nanotech.* **3,** 206–209 (2008).
4. Corso, M. *et al.* Boron nitride nanomesh. *Science* **303,** 217–220 (2004).
5. Morscher, M., Corso, M., Greber, T. & Osterwalder, J. Formation of single layer h-BN on Pd(111). *Surf. Sci.* **600,** 3280–3284 (2006).
6. Goriachko, A. *et al.* Self-assembly of a hexagonal boron nitride nanomesh on Ru(0001). *Langmuir* **23,** 2928–2931 (2007).
7. Kester, D. J., Ailey, K. S., Davis, R. F. & More, K. L. Phase evolution in boron-nitride thin-films. *J. Mater. Res.* **8,** 1213–1216 (1993).
8. Nagashima, A., Tejima, N., Gamou, Y., Kawai, T. & Oshima, C. Electronic dispersion relations of monolayer hexagonal boron nitride formed on the Ni(111) surface. *Phys. Rev. B* **51,** 4606 (1995).
9. Rokuta, E. *et al.* Phonon dispersion of an epitaxial monolayer film of hexagonal boron nitride on Ni(111). *Phys. Rev. Lett.* **79,** 4609 (1997).
10. Levendorf, M. P. *et al.* Graphene and boron nitride lateral heterostructures for atomically thin circuitry. *Nature* **488,** 627–632 (2012).
11. Wang, H. *et al.* BN/graphene/BN transistors for RF applications. *IEEE Electron. Device Lett.* **32,** 1209–1211 (2011).
12. Dean, C. R. *et al.* Boron nitride substrates for high-quality graphene electronics. *Nature Nanotech.* **5,** 722–726 (2010).
13. Britnell, L. *et al.* Field-effect tunneling transistor based on vertical graphene heterostructures. *Science* **335,** 947–950 (2012).
14. Bokdam, M., Khomyakov, P. A., Brocks, G., Zhong, Z. & Kelly, P. J. Electrostatic doping of graphene through ultrathin hexagonal boron nitride films. *Nano Lett.* **11,** 4631–4635 (2011).
15. Decker, R. G. *et al.* Local electronic properties of graphene on a BN substrate via scanning tunneling microscopy. *Nano Lett.* **11,** 2291–2295 (2011).
16. Liu, Z. *et al.* Direct growth of graphene/hexagonal boron nitride stacked layers. *Nano Lett.* **11,** 2032–2037 (2011).
17. Ci, L. *et al.* Atomic layers of hybridized boron nitride and graphene domains. *Nature Mater.* **9,** 430–435 (2010).
18. Song, L. *et al.* Large scale growth and characterization of atomic hexagonal boron nitride layers. *Nano Lett.* **10,** 3209–3215 (2010).
19. Schwierz, F. Graphene transistors. *Nature Nanotech.* **5,** 487–496 (2010).
20. Lee, C. *et al.* Frictional characteristics of atomically thin sheets. *Science* **328,** 76–80 (2010).
21. Choon Sik, C., Lee, J. W. & Jaeheung, K. Dual- and triple-mode branch-line ring resonators and harmonic suppressed half-ring resonators. *IEEE Trans. Microwave Theory Tech.* **54,** 3968–3974 (2006).
22. Grieg, D. D. & Engelmann, H. F. Microstrip—a new transmission technique for the kilomegacycle range. *Proc. IRE* **40,** 1644–1650 (1952).
23. Smith, D. R., Padilla, W. J., Vier, D. C., Nemat-Nasser, S. C. & Schultz, S. Composite medium with simultaneously negative permeability and permittivity. *Phys. Rev. Lett.* **84,** 4184–4187 (2000).
24. Han, S-J. *et al.* High-frequency graphene voltage amplifier. *Nano Lett.* **11,** 3690–3693 (2011).
25. Han, W., Nezich, D., Jing, K. & Palacios, T. Graphene frequency multipliers. *IEEE Electron. Device Lett.* **30,** 547–549 (2009).
26. Qiao, Z., Jung, J., Niu, Q. & MacDonald, A. H. Electronic highways in bilayer graphene. *Nano Lett.* **11,** 3453–3459 (2011).
27. Krivanek, O. L. *et al.* An electron microscope for the aberration-corrected era. *Ultramicroscopy* **108,** 179–195 (2008).

Author contributions

Z.L. designed and carried out most of the experiments (SEM, TEM, Raman, XPS) and analysed the data. L.M. worked on the CVD growth of graphene. Y.G. and K.P.H. conducted the CVD growth of h-BN. G.S. and S.D.L. fabricated graphene/h-BN patterns by photolithography and FIB. W.Z. carried out STEM experiments. J.Z. and J.Y. performed AFM measurements. X.Y. carried out high-frequency measurements of the graphene/h-BN resonator. R.V., J.L. and P.M.A were responsible for project planning. Z.L., K.P.H., W.Z., J-C.I., J.L. and P.M.A. co-wrote the paper. All authors discussed the results.

Additional information

Supplementary information is available in the online version of the paper. Reprints and permission information is available online at http://www.nature.com/reprints. Correspondence and requests for materials should be addressed to J.L. and P.M.A.